


Interaction of orbital angular momentum light with Rydberg excitons: Modifying dipole selection rules

Annika Melissa Konzelmann ¹, Sjard Ole Krüger,² and Harald Giessen^{1,*}

¹*4th Physics Institute and Research Center SCoPE, University of Stuttgart, Pfaffenwaldring 57, D-70569 Stuttgart, Germany*

²*Institut für Physik, Universität Rostock, Albert-Einstein-Straße 23, D-18059 Rostock, Germany*



(Received 17 May 2019; revised manuscript received 26 August 2019; published 17 September 2019;
corrected 6 February 2020)

Orbital angular momentum (OAM) light possesses in addition to its usual helicity ($s = \pm\hbar$, depending on its circular polarization) an orbital angular momentum l . This means that in principle one can transfer more than a single quantum of \hbar during an optical transition from light to a quantum system. However, quantum objects are usually so small (typically in the nanometer range) that they only locally probe the dipolar character of the local electric field. In order to sense the complete macroscopic electric field, we utilize Rydberg excitons in the semiconductor cuprite (Cu_2O), which are single quantum objects of up to micrometer size. Their interaction with focused OAM light allows for matching the focal spot size and the wave-function diameter. Here, the common dipole selection rules ($\Delta j = \pm 1$) should be broken, and transitions of higher Δj with higher-order OAM states should become more probable. Based on group theory, we analyze in detail the optical selection rules governing this process. Then we are able to predict what kind of alternative exciton transitions (quantum number n and l^{exc}) one would expect in absorption spectroscopy on Cu_2O using different kinds of OAM light.

DOI: [10.1103/PhysRevB.100.115308](https://doi.org/10.1103/PhysRevB.100.115308)

I. INTRODUCTION

The giant size of Rydberg atoms leads to huge interaction effects from which one gains insight into atomic physics on the single quantum level [1,2]. In the solid state there exists an analog, called Rydberg exciton, which is an exciton state with large principal quantum number n . This exciton should be capable of sensing elementary excitations in its surroundings on a quantum level [3]. An exciton is an excited state of the crystal, in which an electron and a hole form a quasiparticle bound by Coulomb interaction. In covalent crystals, such as cuprous oxide (Cu_2O), excitons are delocalized, the electron-hole pair is loosely bound, and the orbits are large with macroscopic dimensions of $\sim 1 \mu\text{m}$. The so-called Wannier excitons appear in the low-energy spectrum of the crystal as sharp absorption peaks below the band gap [4]. Excitonic effects are decisive for the optical properties of semiconductors [5], among which cuprous oxide is unique in crystal quality [6]. Rydberg excitons are well suited for the investigation of interaction effects. Huge polarizabilities are expected, leading to enormously strong dipolar interactions [7]. Furthermore, in contrast to Rydberg atoms, highly excited excitons with micrometer-size extensions are of interest because they can be placed and moved in a crystal with high precision using macroscopic energy potential landscapes [8].

The energies of the optically excited excitons can be determined directly by one-photon absorption studies, in which the photon energy of a single-frequency laser with a narrow spectral linewidth of a few neV is continuously tuned. The exciton energy series can be calculated according to

$E_n = E_g - E_B$, with the band-gap energy $E_g = 2.17 \text{ eV}$, the exciton binding energy $E_B = \text{Ry}^*/(n - \delta_{n,l})^2$, the quantum defect $\delta_{n,l}$ induced by the nonparabolic hole dispersions [9], and the modified Rydberg constant [10] $\text{Ry}^* = \text{Ry} m^*/(\epsilon^2 m)$. The crystal environment is taken into account through the permittivity ϵ , which is isotropic for cubic (O_h) symmetry, and the effective electron and hole masses m_e and m_h are incorporated via $m^* = m_e m_h / (m_e + m_h)$.

We are interested in excitons which are formed between the highest valence and lowest conduction bands in cuprous oxide [see Fig. 1(a)]. These bands are formed by copper $3d$ and $4s$ orbitals, respectively. Both bands have the same parity; thus the transition dipole moment for band-to-band transitions vanishes. When forming excitons, only so-called second-class transitions are possible. This means that beyond the valence and conduction band symmetry, also the symmetry of the exciton envelope wave function has to be taken into account. This means that for our case of s - and d -type valence and conduction bands ($\Delta l = 2$), only P excitons with envelope angular momentum $l^{\text{exc}} = 1$ can be excited. In this case, the photon carries one \hbar of angular momentum (right and left circularly polarized light), and the p envelope of the exciton carries the second \hbar of angular momentum that is necessary to make the transition with $\Delta l = 2$ from the $3d$ valence to the $4s$ conduction band. Hence, in Cu_2O , electric dipole transitions cannot lead to excitons with an s -type envelope. However, the transition dipole moment of the second-class transition (p -type envelope) is typically one order of magnitude smaller than for s -type excitons in semiconductors with s - and p -type bands (e.g., GaAs).

All aforementioned considerations are usually done for plane waves with zero *orbital* angular momentum. However, light beams with an azimuthal phase dependence of $e^{-il\varphi}$ carry

*h.giessen@pi4.uni-stuttgart.de; <https://www.pi4.uni-stuttgart.de>

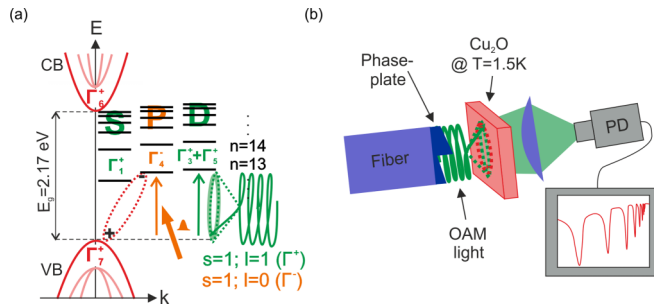


FIG. 1. (a) Formation of different exciton series between the highest valence (VB) and the lowest conduction (CB) bands in Cu_2O depending on the light properties ($s = 1; l = 0, 1$). Using OAM light, Rydberg excitons with different envelope functions (S, P, D, \dots) can be excited by allowed transitions. (b) Experimental scheme: A spiral phase plate imprinted on a fiber facet creates OAM light, which excites Rydberg excitons in cuprite at cryogenic temperatures. The signal is detected using a photodiode (PD). The Rydberg exciton series is visible in the absorption spectrum as broadened, asymmetric, Fano-shaped absorption lines.

an additional orbital angular momentum $l\hbar$, independent of their polarization state [11–15]. For any given l the beam has l intertwined helical phase fronts, for which the Poynting vector has an azimuthal component, meaning it is no longer parallel to the beam axis. That component produces an orbital angular momentum parallel to the beam axis, which is associated with regions of high intensity. This comes together with a phase singularity on the beam axis with zero optical intensity and no linear or angular momentum, which persists no matter how tightly the beam is focused. The most common forms of helically phased beams are the Laguerre-Gauss mode. Such donut modes form a complete basis set for paraxial light beams and have circular symmetry. Orbital angular momentum light can be straightforwardly produced using computer generated holograms [15] or spiral phase plates [16]. In addition, orbital angular momentum (OAM) light carries a strong field gradient in its center while there is no E -field intensity (dark penumbra in the beam center). This unique feature makes the interaction of OAM light with *atomic* matter different from plane waves [17]. In particular, during the interaction of OAM light and atoms one can not only transfer the physical properties of OAM light (spin s and angular momentum l) to internal and external degrees of freedom [18], but one can also use OAM beams to trap particles due to their field gradient [19].

Most importantly, with the combination of OAM light and Rydberg excitons in cuprite (macroscopic quantum objects), we bridge the size gap between light and matter [20]. Previously, Quinteiro studied the excitation of bulk semiconductors by twisted light [21,22]. Time-resolved pump-probe studies using OAM light have been carried out as well [23,24]. Different from atomic physics, the size of the Rydberg excitons, which are single quantum objects, is comparable to the size of a tightly focused OAM beam. In fact, the $n = 25$ Rydberg exciton has a Bohr radius of 920 nm, whereas the wavelength for its excitation is 571 nm, which can be focused down to a tight focus of about 500 nm. This gives us the unique opportunity to investigate the interaction of OAM beams with single quantum objects with comparable sizes in the hundreds-of-nanometer range. In atomic and ionic systems,

the small sizes in the angstrom range probe the OAM beam only locally and thus experience a local field with mostly dipolar character.

When we regard crystals as macroscopic continua, the rotational symmetry is broken down to discrete groups [25]. However, in cuprous oxide this rotational symmetry is still quite high (point group O_h). The symmetry transformations of a Hamiltonian always form a group, which is directly related to the physical symmetry of the system to which the Hamiltonian applies. Such symmetry considerations can be used to extract information residing in the respective transition matrix elements regarding the selection rules associated with orbital angular momentum transfer. Optical transitions occur from the crystal ground state to the excitonic states and are driven by the light field operator. Exciting matter with OAM light allows for one more degree of freedom (spin *and* angular momentum quantum number) compared to usual dipolar light (spin quantum number only). Applied to Rydberg excitons, which can be in different angular momentum quantum states, we can engineer alternative selection rules with OAM light, thus having a rich set of control parameters [26].

II. METHODS

Our aim is to predict whether an optical transition between the cuprite crystal ground state and exciton states with different amounts of angular momentum l^{exc} is allowed or forbidden when exciting with OAM light. For allowed transitions the overlap of crystal ground and excited states contains the symmetry of the exciting light (optical transition driving operator $\mathbf{A} \cdot \mathbf{p}$). The symmetries of the excitonic states are derived from the cuprous oxide band symmetries. As the excitation takes place inside the crystal, we use the tables of Ref. [27] in order to determine the OAM light symmetries within the symmetry group of cuprite.

Cuprous oxide belongs to symmetry group O_h , which contains all 24 proper and 24 improper rotations which transform a cube into itself. See the Supplemental Material [28] for a detailed description of this point group. Knowing how the symmetry group behaves under parity, it suffices to take only the symmetry classes with the proper rotations into account. The symmetry of an exciton is described by the product of the symmetries of the conduction band (electron), the valence band (hole), and the envelope function, determining the angular momentum quantum state. The former two symmetries are known from the literature [29] and the latter one can be derived from the atomic orbitals of the hydrogen wave function due to the high symmetry of cuprite [30–32]. Orbital angular momentum light is described by a Laguerre-Gauss mode, which can be decomposed, in the longitudinal dipole approximation, into a plane wave part A_0 times a phase factor $e^{il\varphi}$. While the symmetry of the plane wave part is trivial, in order to extract the symmetry of the phase factor, we decompose the latter one into basis functions, analyze how these basis functions change when undergoing O_h symmetry operations, and calculate the trace of the transformation matrix (characters). For the complete set of characters (one character per symmetry operation) the corresponding light field symmetry can be assigned according to the character tables of group O_h [27].

III. RESULTS AND DISCUSSION

A. OAM light symmetry assignment via calculation of transformation matrix diagonal elements

In the following we are going to assign a symmetry to the optical transition driving operator involving OAM light modes with different amounts of orbital angular momentum l . OAM light is described by a Laguerre-Gauss mode which is a Gaussian beam times an additional phase factor $e^{il\varphi}$. The complete light field operator \mathbf{A} has the following form:

$$\begin{aligned} \mathbf{A}_l(r, \varphi, z) &= \mathbf{A}_0 e^{ikz} \frac{w_0}{w} \exp \left[\frac{-r^2}{w^2} + \frac{ikr^2}{2R} - i(2p + |l| + 1)\phi(z) \right] \\ &\times \left(\frac{\sqrt{2}r}{w} \right)^{|l|} L_p^{|l|} \left(\frac{2r^2}{w^2} \right) e^{il\varphi}, \end{aligned} \quad (1)$$

with \mathbf{A}_0 : light field amplitude; k : wave vector; $w(z)$: beam waist; $w_0 = w(z=0)$; $\phi(z)$: Gouy phase; $R(z)$: radius of curvature; $L_p^{|l|}$: generalized Laguerre polynomial.

We consider in our calculations only the case where the OAM light propagates in the z direction. The exciton is assumed to be located in the vortex center (xy plane), so the overall symmetry is maintained and the r dependence of the mode does not influence the transformational properties. However, as the field gradient in the OAM light beam becomes important for quadrupole transitions, we develop the light field in z . Then, in dipole approximation the Gaussian beam part simplifies to $\mathbf{A}_0 e^{ikz} \approx \mathbf{A}_0 (1 + ikz) \approx \mathbf{A}_0$. From the OAM part, the only relevant factor for symmetry considerations is $e^{il\varphi}$. Then, the optical transition driving operator becomes $\mathbf{A} \cdot \mathbf{p} = \mathbf{A}_0 e^{il\varphi} \cdot \mathbf{p}$. The symmetries of \mathbf{A}_0 and \mathbf{p} with respect to group O_h are Γ_1^+ and Γ_4^- , respectively. The function $e^{il\varphi}$ is cylindrically symmetric and can be aligned along the three coordinate axes in the cubic cuprite crystal. Thus, we consider the six linearly independent basis functions $e^{+il\varphi_x}$, $e^{-il\varphi_x}$, $e^{+il\varphi_y}$, $e^{-il\varphi_y}$, $e^{+il\varphi_z}$, $e^{-il\varphi_z}$, into which $e^{il\varphi}$ can be transformed under the symmetry operations of point group O_h . For an orientation along different axes, the number of linearly independent basis functions would differ; thus the following analysis only holds strictly for the case in which the beam axis aligns with a coordinate axis. In order to determine the symmetry of function $e^{il\varphi}$, we analyze how the basis functions change when undergoing O_h symmetry operations, and calculate the trace of the transformation matrix (characters). For the complete set of characters, the corresponding symmetry can be assigned according to the character tables of group O_h . The case $l=0$ needs to be considered separately. As $e^{i(l=0)\varphi} = 1$, we cannot find six linear independent basis functions, contrary to the case $l > 0$. The symmetry for the dipolar light field ($l=0$) is Γ_1^+ .

A coordinate transformation of order n leads to the original coordinate after performing the transformation n times, i.e., three times for the eight threefold symmetry axes $8C_3$ of group O_h : $x \rightarrow y \rightarrow z \rightarrow x$. It suffices to select one element per class, i.e., axis (111) in class $8C_3$, as all elements of the same class transform the same way. In contrast, it is important to perform the symmetry considerations for a complete basis, i.e., x , y , and z , in order to extract the character of a

TABLE I. Transformations of functions $e^{\pm il\varphi_x}$, $e^{\pm il\varphi_y}$, and $e^{\pm il\varphi_z}$ under O_h symmetry operations.

Operator \hat{O}	$\hat{O} e^{\pm il\varphi_x}\rangle$	$\hat{O} e^{\pm il\varphi_y}\rangle$	$\hat{O} e^{\pm il\varphi_z}\rangle$
E	$e^{\pm il\varphi_x}$	$e^{\pm il\varphi_y}$	$e^{\pm il\varphi_z}$
$8C_3$	$e^{\pm il\varphi_z}$	$e^{\pm il\varphi_x}$	$e^{\pm il\varphi_y}$
$3C_2$	$e^{\pm il(\varphi_x+\pi)}$	$e^{\mp il(\varphi_y+\pi)}$	$e^{\mp il\varphi_z}$
$6C_4$	$e^{\pm il(\varphi_x+\pi/2)}$	$e^{\mp il(\varphi_z\pm\pi/2)}$	$e^{\pm il(\varphi_y\mp\pi/2)}$
$6C_2'$	$e^{\pm il(\varphi_y-\pi/2)}$	$e^{\pm il(\varphi_x+\pi/2)}$	$e^{\mp il(\varphi_z-\pi/2)}$

transformation (trace of transformation matrix). The complete transformations of the coordinates x , y , z under symmetry operations of group O_h are listed in Table S1 in the Supplemental Material [28]. Knowing how the coordinates behave under the different symmetry operations, one can write down the transformations of the basis functions of $e^{il\varphi}$ (see Table I).

In order to calculate the transformation matrix diagonal elements, the transformed functions are decomposed into basis vectors according to $\hat{O}|f_i\rangle = \sum_k N_{i,k}|f_k\rangle$. The characters of the OAM light for each symmetry class are then given by the sum of the results of all six basis vectors, i.e., the trace $\chi(\hat{O}) = \text{Tr}(N_{i,k}) = \sum_k N_{k,k}$. The single transformation matrix diagonal elements for one representative class element of all symmetry classes of group O_h as well as the resulting character set for OAM light ($e^{il\varphi}$) are listed in Table S2 in the Supplemental Material [28]. Multiplication of the characters of $e^{il\varphi}$ with the ones of \mathbf{A}_0 yield the character set of the complete OAM light field operator $\mathbf{A} = \mathbf{A}_0 e^{il\varphi}$. The amplitude \mathbf{A}_0 is described by symmetry Γ_1^+ , which acts like a 1 in multiplication (identity). Further multiplication with the characters of the momentum operator \mathbf{p} , which is described by symmetry Γ_4^- , yields the characters of the optical transition driving operator $\mathbf{A} \cdot \mathbf{p}$. The resulting character sets are listed in Table II. The assignment of symmetries is done with the help of the character and multiplication tables for symmetry group O_h . Both tables as well as additional character sets for OAM light with different amounts of orbital angular momentum l as well as their symmetries are listed in the Supplemental Material in Tables S2–S4 [28].

Electric quadrupole transitions require a change of two units of angular momentum ($\Delta j = 2$) in matter and are sensitive to the light field gradient $\nabla \mathbf{E}$. Usually, optical beams have a longitudinal field gradient, which allows for driving electric quadrupole transitions, however, with a strength of three orders of magnitude weaker than the electric dipole transition. A transverse gradient, due to the spatial structure of the beam front, such as in OAM light, can drive quadrupole

TABLE II. Character set for OAM light field operator ($\mathbf{A} = \mathbf{A}_0 e^{il\varphi}$) and first-class (dipole, $\mathbf{A} \cdot \mathbf{p} = \mathbf{A}_0 e^{il\varphi} \cdot \mathbf{p}$) and second-class ($\mathbf{A} \cdot \mathbf{p} = \mathbf{A}_0 \cdot ikz e^{il\varphi} \cdot \mathbf{p}$) transition driving operator for OAM light with arbitrary amount of angular momentum l .

O_h	E	$8C_3$	$3C_2$	$6C_4$	$6C_2'$
$\mathbf{A} = \mathbf{A}_0 e^{il\varphi}$	6	0	$2(-1)^l$	$2\cos(l\pi/2)$	0
$\mathbf{A} \cdot \mathbf{p}$ (First class)	18	0	$-2(-1)^l$	$2\cos(l\pi/2)$	0
$\mathbf{A} \cdot \mathbf{p}$ (Second class)	54	0	$2(-1)^l$	$2\cos(l\pi/2)$	0

TABLE III. Exciton envelope (Γ_{env}^l) and total exciton transition (Γ_{exc}) symmetries [32,43,44].

Envelope l^{exc}	Exciton envelope symmetry $\Gamma_{\text{env}}^{l^{\text{exc}}}$	Exciton total symmetry Γ_{exc}
S ($l^{\text{exc}} = 0$)	Γ_1^+	$\Gamma_2^+ + \Gamma_5^+$
P ($l^{\text{exc}} = 1$)	Γ_4^-	$\Gamma_2^- + \Gamma_3^- + \Gamma_4^- + 2\Gamma_5^-$
D ($l^{\text{exc}} = 2$)	$\Gamma_3^+ + \Gamma_5^+$	$\Gamma_1^+ + 2\Gamma_3^+ + 3\Gamma_4^+ + \Gamma_5^+$
F ($l^{\text{exc}} = 3$)	$\Gamma_2^- + \Gamma_4^- + \Gamma_5^-$	$2\Gamma_1^- + \Gamma_2^- + 2\Gamma_3^- + 4\Gamma_4^- + 3\Gamma_5^-$
G ($l^{\text{exc}} = 4$)	$\Gamma_1^+ + \Gamma_3^+ + \Gamma_4^+ + \Gamma_5^+$	$\Gamma_1^+ + 2\Gamma_2^+ + 3\Gamma_3^+ + 4\Gamma_4^+ + 5\Gamma_5^+$

transitions, too [17,33–37]. However, to make $\Delta j > 1$ transitions similar in magnitude to standard electric dipole transitions ($\Delta j = 1$), an atom usually has to be placed precisely in the vortex center (no further than an atomic size a_0) and the probe beam has to be focused close to the diffraction limit. In contrast, the micrometer length scales of Rydberg excitons in cuprite and focused OAM beams match, hence allowing for the realization of enhanced quadrupole transitions triggered by the transverse field gradient in the center of the OAM beam [see Fig. 1(b)] [38]. In order to predict whether such a second-class transition in excitons is allowed using OAM light, the symmetries of the optical transition driving operator are multiplied with the symmetry Γ_4^- , which accounts for the additional position vector in the quadrupole field. However, this way, we obtain the symmetry set for all second-class transitions, meaning including also magnetic-dipole transitions, resulting for $l = 0$ into $\Gamma_1^+ + \Gamma_3^+ + \Gamma_4^+ + \Gamma_5^+$. From Ref. [28] we know that the only possible quadrupole transitions are of symmetry Γ_3^+ and Γ_5^+ . The resulting character sets for first- and second-class transitions for an arbitrary amount of orbital angular momentum l are listed in Table II. More detailed information can be found in Table S2 in the Supplemental Material [28].

B. Symmetry of excitons in cuprous oxide

The total symmetry of an exciton is determined by the product of valence band (hole), conduction band (electron), and envelope function (angular momentum l^{exc}) symmetries: $\Gamma_{\text{exc}} = \Gamma_h \times \Gamma_e \times \Gamma_{\text{env}}$. In cuprous oxide, the electronic configurations of the single atoms (Cu and O) determine that conduction and valence bands are mainly formed from the Cu $4s$ and Cu $3d$ functions, respectively [29,39,40]. In the crystal field the Cu $4s$ conduction band obtains symmetry Γ_1^+ . The Cu $3d$ valence band splits into an energetically higher-lying, threefold degenerate band of symmetry Γ_5^+ and a lower-lying, twofold degenerate band of symmetry Γ_3^+ . Due to the spin-orbit coupling between the quasispin I and the hole spin

S_h , the now sixfold (including spin) degenerate Γ_5^+ valence band splits into a higher-lying twofold degenerate band of symmetry Γ_7^+ and a lower-lying fourfold degenerate band of symmetry Γ_8^+ by an amount of $\Delta = 130$ meV [41]. Including spin, the Γ_1^+ conduction band is now twofold degenerate and described by symmetry Γ_6^+ . We consider here the yellow exciton series which occurs between the uppermost valence band (Γ_7^+) and the lowest conduction band (Γ_6^+) [see Fig. 1(a)]; thus $\Gamma_{\text{exc}} = \Gamma_h \times \Gamma_e \times \Gamma_{\text{env}} = \Gamma_7^+ \times \Gamma_6^+ \times \Gamma_{\text{env}}^{l^{\text{exc}}}$.

The symmetry property of the pure Coulomb field between electron and hole gives rise to the degeneracy of all levels with the same principal quantum number n irrespective of their angular momentum quantum number l^{exc} , which is described by the exciton envelope function, expressed in spherical harmonic functions Y_l^m [42]. These are listed in Table S5 in the Supplemental Material [28] in Cartesian coordinates for $l^{\text{exc}} = 0 \dots 4$. It suffices to use one representative function per orbital (symmetry group), i.e., choosing one magnetic quantum number value m , Y_0^0 for S or Y_1^1 for P , to perform symmetry considerations. In the simplest case, the orbital functions are pure basis functions, so their symmetry can be directly assigned according to the character table of symmetry group O_h . The orbital functions are then irreducible representations, which is the case for S and P orbitals: $Y_0^0 = 1/\sqrt{4\pi} \sim 1 \rightarrow S$ orbital transforms as Γ_1^+ ; $Y_1^1 = -\sqrt{3}/8\pi(x-iy)/r \rightarrow P$ orbital transforms as Γ_4^- . If the bases cannot be seen directly, one has to apply the different symmetry operations of group O_h to the orbital function and decompose them via $N_{m_1, m_2} = \langle Y_1^{m_1} | \hat{O} | Y_1^{m_2} \rangle$, yielding the complete character sets (shown in Table S6 in the Supplemental Material) [28]. The resulting orbital symmetries, known via comparison of the character sets with the O_h character table, are shown in Table III together with the complete exciton symmetries for different envelope functions. In addition, the crystal ground state has symmetry Γ_1^+ . Therefore the transition may be allowed if the symmetry of the excitonic state appears in the decomposition of the optical transition driving operator.

TABLE IV. Symmetries of dipole and quadrupole transition driving operator of OAM light with different amounts of orbital angular momentum l .

Orbital angular momentum l	Dipole	Quadrupole
0 (Even)	Γ_4^-	$\Gamma_3^+ + \Gamma_5^+$
1 (Odd)	$\Gamma_1^+ + \Gamma_2^+ + 2\Gamma_3^+ + 2\Gamma_4^+ + 2\Gamma_5^+$	$\Gamma_1^- + \Gamma_2^- + 2\Gamma_3^- + 4\Gamma_4^- + 4\Gamma_5^-$
2 (Even)	$\Gamma_2^- + \Gamma_3^- + 2\Gamma_4^- + 3\Gamma_5^-$	$2\Gamma_1^+ + \Gamma_2^+ + 3\Gamma_3^+ + 4\Gamma_4^+ + 3\Gamma_5^+$
3 (Odd)	$\Gamma_1^+ + \Gamma_2^+ + 2\Gamma_3^+ + 2\Gamma_4^+ + 2\Gamma_5^+$	$\Gamma_1^- + \Gamma_2^- + 2\Gamma_3^- + 4\Gamma_4^- + 4\Gamma_5^-$
4 (Even)	$\Gamma_1^- + \Gamma_3^- + 3\Gamma_4^- + 2\Gamma_5^-$	$\Gamma_1^+ + 2\Gamma_2^+ + 3\Gamma_3^+ + 3\Gamma_4^+ + 4\Gamma_5^+$

TABLE V. Exciton transition symmetries and OAM light with which they can be excited.

Envelope l^{exc}	Exciton total symmetry Γ_{exc}	Parity	l^{dipole}	$l^{\text{quadrupole}}$
<i>S</i>	$\Gamma_2^+ + \Gamma_5^+$	+	Odd	Even
<i>P</i>	$\Gamma_2^- + \Gamma_3^- + \Gamma_4^- + 2\Gamma_5^-$	-	Even	Odd
<i>D</i>	$\Gamma_1^+ + 2\Gamma_3^+ + 3\Gamma_4^+ + \Gamma_5^+$	+	Odd	Even
<i>F</i>	$2\Gamma_1^- + \Gamma_2^- + 2\Gamma_3^- + 4\Gamma_4^- + 3\Gamma_5^-$	-	Even	Odd
<i>G</i>	$\Gamma_1^+ + 2\Gamma_2^+ + 3\Gamma_3^+ + 4\Gamma_4^+ + 5\Gamma_5^+$	+	Odd	Even
<i>H</i>	$\Gamma_1^- + 2\Gamma_2^- + 4\Gamma_3^- + 5\Gamma_4^- + 6\Gamma_5^-$	-	Even	Odd

C. Interaction of OAM light with Rydberg excitons: Modifying dipole selection rules

In Table IV the different light field operators for dipole and quadrupole OAM light are summarized. “ $l = 1$ ” and “ $l = 3$ ” OAM light exhibit the same symmetry. If the dipolar light field operator is of positive parity, the corresponding quadrupole light field operator is of negative parity and vice versa. For successive increase of OAM l , the parity changes alternatively. When illuminating cuprous oxide with dipolar light ($l = 0$), *P* excitons are visible in the absorption spectrum. According to our calculations *P* excitons can also become allowed transitions in quadrupole excitation using $l = 1$ or $l = 3$ OAM light. In contrast, the usually dipole-forbidden *S*-exciton states can not only be driven by the quadrupole field of even OAM light ($l = 0, 2, 4$), but also by dipole transitions with odd OAM light ($l = 1, 3$). The same holds for *D* and *G* excitons, while *F* and *H* excitons follow the excitation rules of *P* excitons. These results are summarized in Table V.

D. Exciton and light mode spatial extensions

We would like to predict for which principal quantum number n a Rydberg exciton in cuprous oxide would most likely interact with focused OAM light, due to their largest spatial overlap. Therefore, the *S*-exciton envelope wave functions are visualized as a function of n and their spatial overlap with a light mode of $l = 1$ orbital angular momentum is discussed. The excitonic radial wave function $r^2 R_{\text{Cu}_2\text{O}}^2(r)$ is calculated in analogy to the hydrogen radial wave function R_{nl} and the light mode spatial extension is calculated based on the formula for Laguerre-Gauss modes for $l = 1$ at the focal point $z = 0$:

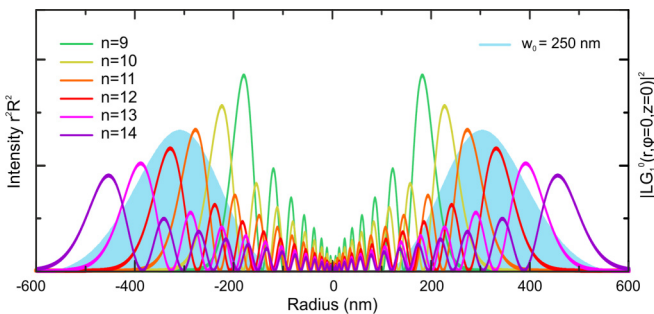


FIG. 2. Visualization of the spatial overlap between exciton states and a Laguerre-Gauss mode. The *S*-exciton ($l^{\text{exc}} = 0$) radial wave function $r^2 R_{\text{Cu}_2\text{O}}^2(r)$ is plotted for different quantum states $n = 9 \dots 14$. The intensity distribution of the Laguerre-Gauss mode ($l = 1$) is shown for a beam waist $w_0 = 250$ nm.

$|u_{l=1}^{p=0}(r, \varphi = 0, z = 0)|^2$. The results are shown in Fig. 2 for *S*-exciton states with principal quantum number $n = 9 \dots 14$. From here we see that *S*-exciton states with principal quantum number $n = 12$ show the largest overlap with the spatial mode of $l = 1$ OAM light when focused down to a spot of $w_0 = 250$ nm beam waist, which corresponds to a radius $r = 497$ nm. See the Supplemental Material for more details [28].

IV. CONCLUSION AND OUTLOOK

In the present paper we have given a detailed analysis of orbital angular momentum (OAM) light and exciton symmetries in cuprite. The symmetries of OAM light with different amounts of OAM l as well as the symmetries of excitons with different envelope functions (angular momentum quantum number l^{exc}) have been calculated. Comparing their overlap with the dipole selection rules allows us to predict that the alteration of the OAM of light may enable one to modify the optical transition selection rules and, hence, to excite usually dipole-forbidden Rydberg excitons in Cu_2O . We find that *s*- and *d*-envelope wave-function excitons should be excitable with $l = 1$ and $l = 3$ OAM light. The precise oscillator strength of the transitions, however, requires further detailed theoretical investigation, meaning elaborate numerical calculations, taking the exact band structure, the exciton envelope wave function, and the exact spatial shape and extension of the OAM beam into account. However, it has been shown that the normally weak optical quadrupole interaction in *atoms* is enhanced significantly when the atom interacts at near resonance with an optical vortex [35]. Furthermore, transition amplitudes have been calculated for excitation of hydrogen-like atoms by OAM light [34]. If the target atom is located at distances of the order of atomic size near the phase singularity in the vortex center, the transition rates into states with OAM $l > 1$ become comparable with the rates for electric dipole transitions. As the Rydberg exciton is located in the center of the OAM beam and senses its complete light field, we assume the effect to be substantially enhanced in solids as well.

Using group-theoretical methods, we propose a method for the observation of dipole-forbidden excitons in cuprite. In order to test the predictions we would like to implement the corresponding experiment as follows [see Fig. 1(b)]: Orbital angular momentum light can be created by imprinting a phase plate on a fiber facet [45]. Upon transmission through the phase plate, a beam of wavelength λ is subjected to a phase delay ψ which depends on the azimuthal angle φ , where $\psi = (n_{pp} - n_0)s\varphi/\lambda$ (s : step height; n_0/n_{pp} : refractive index of the surrounding material and phase plate, respectively). A

screw phase dislocation produced on axis causes destructive interference leading to the characteristic ring intensity pattern in the far field. For a pure Laguerre-Gauss mode the total phase delay around the phase plate must be an integer multiple of 2π ; thus the physical step height in the spiral phase plate is given by $s = l\lambda/(n_{pp} - n_0)$. The purity of Laguerre-Gauss modes is limited by the coproduction of higher-order modes. This OAM light is then focused, for example, by a Fresnel lens carved into the Cu_2O crystal, and transmission measurements are performed. We are going to analyze the different transition probabilities as a set of quantum number n and exciton envelope wave function (angular momentum quantum number l^{exc}), as well as orbital angular momentum quantum number l . In addition, we want to calculate the transition matrix elements and oscillator strength using DFT. Then we would also be able to predict how probable an allowed transition will be.

Overall, only a few experiments have been conducted so far with macroscopic Rydberg excitons in cuprite. Using OAM light will modify their absorption spectrum. In particular, not many studies have investigated D excitons ($l = 2$) in detail in contrast to S and P excitons [7,32,46,47]. Furthermore, more work needs to be done on experiments that combine OAM light and macroscopic quantum objects, such as the Rydberg excitons in Cu_2O .

ACKNOWLEDGMENTS

We gratefully acknowledge funding by the Deutsche Forschungsgemeinschaft (DFG) (SPP 1929 GiRyd) and the European Research Council (ERC) (Complexplas). Discussions with T. Pfau, M. M. Glazov, and J. Heckötter are acknowledged.

-
- [1] T. F. Gallagher, Rydberg atoms, *Rep. Prog. Phys.* **51**, 143 (1988).
- [2] M. Saffman, T. G. Walker, and K. Mølmer, Quantum information with Rydberg atoms, *Rev. Mod. Phys.* **82**, 2313 (2010).
- [3] V. Walther, S. O. Krüger, S. Scheel, and T. Pohl, Interactions between Rydberg excitons in Cu_2O , *Phys. Rev. B* **98**, 165201 (2018).
- [4] J. L. Deiss and A. Daunois, Modulated exciton spectroscopy, *Surf. Sci.* **37**, 804 (1973).
- [5] C. F. Klingshirm, *Semiconductor Optics* (Springer, Berlin, 2012).
- [6] E. F. Gross, Optical spectrum of excitons in the crystal lattice, *Nuovo Cimento* **3** (Suppl. 4), 672 (1956).
- [7] T. Kazimierzczuk, D. Fröhlich, S. Scheel, H. Stolz, and M. Bayer, Giant Rydberg excitons in the copper oxide Cu_2O , *Nature* **514**, 343 (2014).
- [8] S. O. Krüger and S. Scheel, Waveguides for Rydberg excitons in Cu_2O from strain traps, *Phys. Rev. B* **97**, 205208 (2018).
- [9] F. Schöne, S.-O. Krüger, P. Grünwald, M. Aßmann, J. Heckötter, J. Thewes, H. Stolz, D. Fröhlich, M. Bayer, and S. Scheel, Coupled valence band dispersions and the quantum defect of excitons in Cu_2O , *J. Phys. B* **49**, 134003 (2016).
- [10] G. M. Kavoulakis, Y.-Ch. Chang, and G. Baym, Fine structure of excitons in Cu_2O , *Phys. Rev. B* **55**, 7593 (1997).
- [11] N. B. Simpson, K. Dholakia, L. Allen, and M. J. Padgett, Mechanical equivalence of spin and orbital angular momentum of light: an optical spanner, *Opt. Lett.* **22**, 52 (1997).
- [12] M. Padgett, J. Courtial, and L. Allen, Light's orbital angular momentum, *Phys. Today* **57** (5), 35 (2004).
- [13] Y. Yan and A. E. Willner, Efficient generation and multiplexing of optical orbital angular momentum modes in a ring fiber by using multiple coherent inputs, *Opt. Lett.* **37**, 3645 (2012).
- [14] G. A. Turnbull, D. A. Robertson, G. M. Smith, L. Allen, and M. J. Padgett, The generation of free-space Laguerre-Gaussian modes at millimetre-wave frequencies by use of a spiral phase plate, *Opt. Commun.* **127**, 183 (1996).
- [15] N. R. Heckenberg, R. McDuff, C. P. Smith, H. Rubinsztein-Dunlop, and M. J. Wegener, Laser beams with phase singularities, *Opt. Quantum Electron.* **24**, S951 (1992).
- [16] M. W. Beijersbergen, R. P. C. Coerwinkel, M. Kristensen, and J. P. Woerdman, Helical-wavefront laser beams produced with a spiral phaseplate, *Opt. Commun.* **112**, 321 (1994).
- [17] Ch. T. Schmiegelow, J. Schulz, H. Kaufmann, T. Ruster, U. G. Poschinger, and F. Schmidt-Kaler, Transfer of optical orbital angular momentum to a bound electron, *Nat. Commun.* **7**, 12998 (2016).
- [18] A. Afanasev, C. E. Carlson, and A. Mukherjee, Two properties of twisted-light absorption, *J. Opt. Soc. Am. B* **31**, 2721 (2014).
- [19] A. Ashkin and J. M. Dziedzic, Stability of optical levitation by radiation pressure, *Appl. Phys. Lett.* **24**, 586 (1974).
- [20] N. Rivera, I. Kaminer, B. Zhen, J. D. Joannopoulos, and M. Soljačić, Shrinking light to allow forbidden transitions on the atomic scale, *Science* **353**, 263 (2016).
- [21] G. F. Quinteiro, Below-bandgap excitation of bulk semiconductors by twisted light, *Europhys. Lett.* **91**, 27002 (2010).
- [22] G. F. Quinteiro and P. I. Tamborenea, Theory of the optical absorption of light carrying orbital angular momentum by semiconductors, *Europhys. Lett.* **85**, 47001 (2009).
- [23] M. A. Noyan and J. M. Kikkawa, Time-resolved orbital angular momentum spectroscopy, *Appl. Phys. Lett.* **107**, 032406 (2015).
- [24] K. Shigematsu, K. Yamane, R. Morita, and Y. Toda, Coherent dynamics of exciton orbital angular momentum transferred by optical vortex pulses, *Phys. Rev. B* **93**, 045205 (2016).
- [25] T. Inui, Y. Tanabe, and Y. Onodera, *Group Theory and its Applications in Physics* (Springer, Berlin, 1996).
- [26] F. Machado, N. Rivera, H. Buljan, M. Soljačić, and I. Kaminer, Shaping polaritons to reshape selection rules, *ACS Photonics* **5**, 3064 (2017).
- [27] G. F. Koster, J. O. Dimmock, R. G. Wheeler, and H. Statz, *Properties of the Thirty-Two Point Groups*, The MIT Press Research Monographs (The MIT Press, Cambridge, MA, 1963).
- [28] See Supplemental Material at <http://link.aps.org/supplemental/10.1103/PhysRevB.100.115308> for more details on coordinate transformations under symmetry group O_h , as well as exciton envelope functions and exciton and light mode spatial extensions.
- [29] R. J. Elliott, Symmetry of excitons in Cu_2O , *Phys. Rev.* **124**, 340 (1961).

- [30] R. S. Knox and A. Gold, *Symmetry in the Solid State* (W. A. Benjamin, Inc., New York, 1964).
- [31] A. Werner and H. D. Hochheimer, High-pressure x-ray study of Cu_2O and Ag_2O , *Phys. Rev. B* **25**, 5929 (1982).
- [32] J. Thewes, J. Heckötter, T. Kazimierczuk, M. Aßmann, D. Fröhlich, M. Bayer, M. A. Semina, and M. M. Glazov, Observation of High Angular Momentum Excitons in Cuprous Oxide, *Phys. Rev. Lett.* **115**, 027402 (2015).
- [33] S. Franke-Arnold, Optical angular momentum and atoms, *Philos. Trans. R. Soc., A* **375**, 20150435 (2017).
- [34] A. Afanasev, High-multipole excitations of hydrogen-like atoms by twisted photons near a phase singularity, *J. Opt.* **18**, 074013 (2016).
- [35] V. E. Lembessis and M. Babiker, Enhanced Quadrupole Effects for Atoms in Optical Vortices, *Phys. Rev. Lett.* **110**, 083002 (2013).
- [36] S. M. Lloyd, M. Babiker, and J. Yuan, Interaction of electron vortices and optical vortices with matter and processes of orbital angular momentum exchange, *Phys. Rev. A* **86**, 023816 (2012).
- [37] G. F. Quinteiro, F. Schmidt-Kaler, and C. T. Schmiegelow, Twisted-Light-Ion Interaction: The Role of Longitudinal Fields, *Phys. Rev. Lett.* **119**, 253203 (2017).
- [38] A. Syouji, S. Saito, and A. Otomo, Creation of excitons excited by light with a spatial mode, *J. Phys. Soc. Jpn.* **86**, 124720 (2017).
- [39] J. W. Hodby, T. E. Jenkins, C. Schwab, H. Tamura, and D. Trivich, Cyclotron resonance of electrons and of holes in cuprous oxide, Cu_2O , *J. Phys. C* **9**, 1429 (1976).
- [40] K. Suzuki and J. C. Hensel, Quantum resonances in the valence bands of germanium, *Phys. Rev. B* **9**, 4184 (1974).
- [41] F. Schweiner, J. Main, G. Wunner, M. Freitag, J. Heckötter, Ch. Uihlein, M. Aßmann, D. Fröhlich, and M. Bayer, Magnetoexcitons in cuprous oxide, *Phys. Rev. B* **95**, 035202 (2017).
- [42] V. Heine, *Group Theory in Quantum Mechanics* (Pergamon, Oxford, 1960).
- [43] J. C. Merle, C. Wecker, A. Daunois, J. L. Deiss, and S. Nikitine, Modulated excitonic absorption on Cu_2O in magnetic or parallel electric and magnetic fields, *Surf. Sci.* **37**, 347 (1973).
- [44] J. Heckötter, M. Freitag, D. Fröhlich, M. Aßmann, M. Bayer, M. A. Semina, and M. M. Glazov, High resolution study of the yellow excitons in Cu_2O subject to an electric field, *Phys. Rev. B* **95**, 035210 (2017).
- [45] K. Weber, F. Hütt, S. Thiele, T. Gissibl, A. Herkommer, and H. Giessen, Single mode fiber based delivery of OAM light by 3D direct laser writing, *Opt. Express* **25**, 19672 (2017).
- [46] D. Fröhlich, R. Kenklies, Ch. Uihlein, and C. Schwab, Assignment of the Even-Parity Excitons in Cu_2O , *Phys. Rev. Lett.* **43**, 1260 (1979).
- [47] J. Mund, D. Fröhlich, D. R. Yakovlev, and M. Bayer, High-resolution second harmonic generation spectroscopy with femtosecond laser pulses on excitons in Cu_2O , *Phys. Rev. B* **98**, 085203 (2018).

Correction: Four references and their citations in Sec. I were missing and have been inserted.